Numerical analyses of the sound absorption of cylindrical microperforated panel space absorbers with cores

Toyoda, Masahiro
Fujita, Shota
Sakagami, Kimihiro

(Citation)
The Journal of the Acoustical Society of America,138(6):3531-3531

(Issue Date)
2015-12-10

(Resource Type)
journal article

(Version)
Version of Record

Numerical analyses of the sound absorption of cylindrical microperforated panel space absorbers with cores

Masahiro Toyoda,[1,a)] Shota Fujita,[2] and Kimihiro Sakagami[2]
[1]*Department of Architecture, Faculty of Environmental and Urban Engineering, Kansai University, 3-3-35, Yamate-cho, Suita-shi, Osaka, 564-8680, Japan*
[2]*Environmental Acoustics Laboratory, Department of Architecture, Graduate School of Engineering, Kobe University, Rokko, Nada, Kobe, 657-8501, Japan*

(Received 8 July 2015; revised 29 October 2015; accepted 13 November 2015; published online 10 December 2015)

Microperforated panels (MPPs) are next-generation absorption materials because they can provide wideband sound absorption without fibrous materials and can be composed of diverse materials to meet global environmental demands. The fundamental absorbing mechanism is Helmholtz-resonance absorption due to perforations and an air cavity. MPPs are typically backed by rigid flat walls, but to reduce the restrictions on the MPP absorber properties, one of the authors has proposed MPP space sound absorbers without backing structures, including three-dimensional cylindrical microperforated panel space absorbers (CMSAs). Advantages of MPPs without backing structures are design flexibility and ease of use. Besides, the absorption characteristics of a CMSA with a core, which has a rigid cylindrical core inside the CMSA, have been experimentally tested, but a method to predict the absorption characteristics is necessary to design CMSAs with cores. Herein the two-dimensional combined Helmholtz integral formulation method is employed, and its prediction accuracy is evaluated by comparing the measured and predicted absorption characteristics of a CMSA with a core. Furthermore, a parametric study with regard to the core size is carried out to investigate the transition of the absorbing mechanism.
 [http://dx.doi.org/10.1121/1.4936944]

[NX] Pages: 3531–3538

I. INTRODUCTION

A microperforated panel (MPP) is a thin panel or film with submillimeter holes and a perforation ratio less than 1%. MPPs provide better sound absorption performances than ordinary perforated panels with larger apertures because the acoustic resistance and reactance are appropriately tuned for sound absorption. Since Maa first proposed the concept of an MPP,[1] its design principles as well as its effectiveness have been studied.[2–4] Currently, MPP absorbers are recognized as next-generation absorption materials because they can provide wideband sound absorption without fibrous or porous materials and can be composed of diverse materials to meet global environmental demands.

Because the fundamental absorbing mechanism of an MPP absorber is Helmholtz-resonance absorption due to perforations and an air-back cavity, the basic setup involves an MPP backed by a rigid flat wall. MPP absorbers have been applied to various practical problems, for example, in communication rooms,[5] auditoriums,[6] windows,[7] duct silencers,[8–11] cylinders,[12] and noise barriers.[13] To improve the absorption performance, irregular shaped backings[14–17] or electromechanical approaches[18–21] have been suggested and the applicability of an MPP absorber is even now expanded. As for an MPP itself, effects of the hole shape have been investigated with the techniques of computational fluid dynamics[22,23] and the vibroacoustic behaviors have also been studied in detail and utilized to enhance the performance.[24–27] Furthermore, characterization methods for the surface impedance of an MPP structure have been proposed[28,29] and then the prediction of the practical performance in actual environments becomes more precise.

However, to remove the usage restriction due to a back wall, one of the authors has proposed MPP space sound absorbers without backing structures. As a basic form of such MPP space absorbers, multiple-leaf MPP structures without a back wall have been proposed.[30–33] Double-leaf microperforated panel space absorbers (DLMPPs) have an air cavity but without a rigid back wall and triple-leaf microperforated panel space absorbers (TLMPPs) have similar structures to those of DLMPPs. The sound absorption characteristics and the effectiveness of these sound-absorbing structures have been examined theoretically and experimentally. However, the flat panel-like structures of DLMPPs and TLMPPs may restrict their practical uses in actual rooms or buildings.

To expand the applicability and designs of MPP space absorbers, one of the authors has proposed three-dimensional cylindrical MPP space absorbers (CMSAs)[34] and rectangular MPP space absorbers (RMSAs).[35] A CMSA (RMSA) is comprised of an MPP in a cylindrical (rectangular) shape. Design advantages include flexibility and ease of use. These space absorbers can be placed freely on a floor or hung from a ceiling. CMSAs and RMSAs show moderate sound absorption

[a)]Electronic mail: toyoda@kansai-u.ac.jp

over wideband frequencies and their absorption characteristics can be predicted by the two-dimensional boundary element method.[36]

In addition, the absorption characteristics of a CMSA with a core, which has a rigid cylindrical core inside a CMSA, have been experimentally tested.[37] When the core diameter is small, a CMSA with a core has a performance similar to that of a CMSA. However, when the core diameter is large, its performance is similar to a typical rigid-backed MPP. This means that a CMSA with a core can be used effectively by adjusting the core diameter to absorb sound energy at the target frequency.

To efficiently design CMSAs with a core, a calculation method must be developed to predict the absorption characteristics, especially the peak frequency of a CMSA with a core.[37] Herein the two-dimensional combined Helmholtz integral equation formulation (CHIEF) method[38] is employed to predict the absorption characteristics. The prediction accuracy is evaluated by comparing the measured and predicted absorption characteristics of a CMSA with a core. Furthermore, a parametric study with regard to the core size is conducted to investigate the transition of the absorbing mechanism.

II. FORMULATION

A. Model

Two-dimensional prediction models are employed. Although three-dimensional models are better suited for three-dimensional space absorbers (Fig. 1, left), a two-dimensional analysis should be sufficient because MPP structures generally have a higher absorption performance under plane waves with a normal incidence rather than other angles. In addition, employing a two-dimensional model drastically reduces the required computational resources. Therefore, a two-dimensional cylindrical calculation model for a CMSA with an internal rigid core is considered assuming an incident plane wave with a unit amplitude and incident azimuth angle θ (Fig. 1, right).

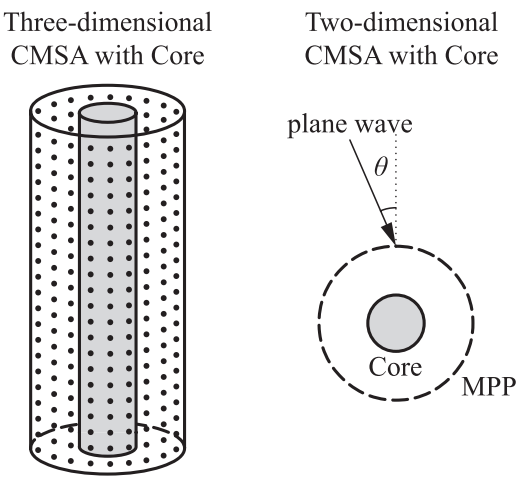

FIG. 1. Three- and two-dimensional models for a CMSA with a core.

B. Boundary integral equation

Region Ω_1 is bounded externally by Σ with center p, which is a sound receiver, and internally by Γ' and small spheres σ_s and σ_p, which have respective centers s and p and small radii ε (Fig. 2), where s is the sound source, q is a point on the boundary, and $\mathbf{n}$ is the inward normal. Transmission admittance ratio A is assumed on Γ', and region Ω_2 is bounded externally by Γ' and internally by Γ'', which is assumed to be a rigid boundary. Region Ω_3 is bounded externally by Γ''. The time factor $\exp(-i\omega t)$ is suppressed throughout, where i is an imaginary unit, ω is the angular frequency, and t is time. Green's identity or integration by parts can be applied to region Ω_1 as

$$\int_{\Omega_1}\left(f\nabla^2 g - g\nabla^2 f\right)dS = \int_{\Sigma+\sigma_s+\sigma_p+\Gamma'}\left(f\frac{\partial g}{\partial \mathbf{n}} - \frac{\partial f}{\partial \mathbf{n}}g\right)d\Gamma, \tag{1}$$

where f and g are continuous and smooth functions. Substituting velocity potential ψ and basic solution G, which satisfy the two-dimensional Helmholtz equation, for f and g, respectively, yields the boundary integral equation for region Ω_1. The basic solution G can be written as

$$G(\mathbf{r}_p,\mathbf{r}_q) = \frac{i}{4}\mathbf{H}_0^{(1)}(kr_{pq}) = \frac{i}{4}\left\{\mathbf{J}_0(kr_{pq}) + i\mathbf{Y}_0(kr_{pq})\right\}, \tag{2}$$

where $\mathbf{r}$ is a position vector, k is the wavenumber, and r_{pq} is the distance between p and q. $\mathbf{H}_0^{(1)}$, $\mathbf{J}_0$, and $\mathbf{Y}_0$ are the Hankel function of the first kind of order zero, the Bessel function of order zero, and Neumann function of order zero, respectively. Taking the limit $\varepsilon \to 0$, the integral over σ_s in Eq. (1) can be written as

$$\int_{\sigma_s}\left\{\psi(\mathbf{r}_q)\frac{\partial G(\mathbf{r}_p,\mathbf{r}_q)}{\partial \mathbf{n}_q} - \frac{\partial \psi(\mathbf{r}_q)}{\partial \mathbf{n}_q}G(\mathbf{r}_p,\mathbf{r}_q)\right\}d\Gamma = \varphi_d(\mathbf{r}_p), \tag{3}$$

where φ_d is the velocity potential due to a direct wave from the sound source. Similarly, the integral over σ_p in Eq. (1) can be expressed as

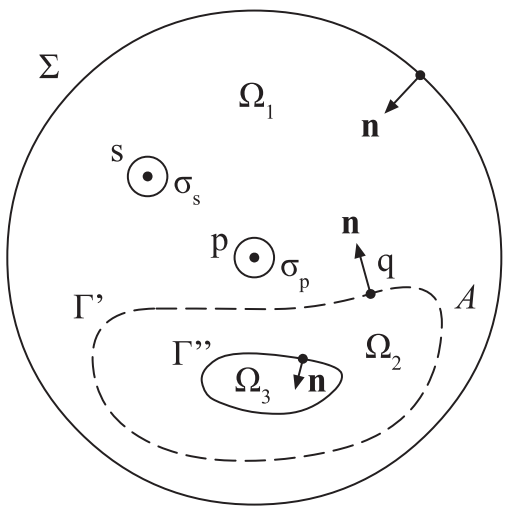

FIG. 2. Two-dimensional model to derive the boundary integral equation.

$$\int_{\sigma_p}\left\{\psi(\mathbf{r}_q)\frac{\partial G(\mathbf{r}_p,\mathbf{r}_q)}{\partial \mathbf{n}_q}-\frac{\partial \psi(\mathbf{r}_q)}{\partial \mathbf{n}_q}G(\mathbf{r}_p,\mathbf{r}_q)\right\}d\Gamma = -C(\mathbf{r}_p)\psi(\mathbf{r}_p), \tag{4}$$

where $C(\mathbf{r}_p)$ is the ratio of the included-part solid angle of σ_p in Ω_1 to 4π; if p is on a smooth boundary, $C(\mathbf{r}_p)=1/2$. Assuming that Σ is a circle with an infinite radius and considering the Sommerfeld radiation condition,[39] which can be expressed as

$$|r_{pq}\psi(\mathbf{r}_q)|<K,\quad \sqrt{r_{pq}}\left\{\frac{\partial\psi(\mathbf{r}_q)}{\partial r_{pq}}-ik\psi(\mathbf{r}_q)\right\}\to 0 \quad (r_{pq}\to\infty), \tag{5}$$

where K is a finite real number, the integral over Σ in Eq. (1) can be neglected. Consequently, substituting Eqs. (3) and (4) into Eq. (1) yields

$$\varphi_d(\mathbf{r}_p)+\int_{\Gamma'}\left\{\varphi_1(\mathbf{r}_q)\frac{\partial G(\mathbf{r}_p,\mathbf{r}_q)}{\partial \mathbf{n}_q}-\frac{\partial\varphi_1(\mathbf{r}_q)}{\partial \mathbf{n}_q}G(\mathbf{r}_p,\mathbf{r}_q)\right\}d\Gamma = \begin{cases}\varphi_1(\mathbf{r}_p) & (p\in\Omega_1)\\ \frac{1}{2}\varphi_1(\mathbf{r}_p) & (p\in\Gamma')\\ 0 & (p\notin\Omega_1,\Gamma')\end{cases} \tag{6}$$

where φ_1 is the velocity potential in Ω_1. Similarly, the equation for region Ω_2 can be obtained as

$$-\int_{\Gamma'+\Gamma''}\left\{\varphi_2(\mathbf{r}_q)\frac{\partial G(\mathbf{r}_p,\mathbf{r}_q)}{\partial \mathbf{n}_q}-\frac{\partial\varphi_2(\mathbf{r}_q)}{\partial \mathbf{n}_q}G(\mathbf{r}_p,\mathbf{r}_q)\right\}d\Gamma = \begin{cases}\varphi_2(\mathbf{r}_p) & (p\in\Omega_2)\\ \frac{1}{2}\varphi_2(\mathbf{r}_p) & (p\in\Gamma',\Gamma'')\\ 0 & (p\notin\Omega_2,\Gamma',\Gamma'')\end{cases} \tag{7}$$

where φ_2 is the velocity potential in Ω_2. Letting $v(\mathbf{r}_q)$ be the velocity in direction $\mathbf{n}$ at q leads to

$$\frac{\partial\varphi_1(\mathbf{r}_q)}{\partial \mathbf{n}_q}=\frac{\partial\varphi_2(\mathbf{r}_q)}{\partial \mathbf{n}_q}=-v(\mathbf{r}_q) = -ikA(\mathbf{r}_q)\{\varphi_1(\mathbf{r}_q)-\varphi_2(\mathbf{r}_q)\}(q\in\Gamma'), \tag{8}$$

$$\frac{\partial\varphi_2(\mathbf{r}_q)}{\partial \mathbf{n}_q}=0\quad(q\in\Gamma''). \tag{9}$$

Considering Eqs. (8) and (9), adding Eqs. (6) and (7) for p on Γ' and Γ'' yields

$$\varphi_d(\mathbf{r}_p)+\int_{\Gamma'}\varphi'(\mathbf{r}_q)\frac{\partial G(\mathbf{r}_p,\mathbf{r}_q)}{\partial \mathbf{n}_q}d\Gamma+\int_{\Gamma''}\varphi''(\mathbf{r}_q)\frac{\partial G(\mathbf{r}_p,\mathbf{r}_q)}{\partial \mathbf{n}_q}d\Gamma = \begin{cases}\frac{1}{2}\{\varphi_1(\mathbf{r}_p)+\varphi_2(\mathbf{r}_p)\} & (p\in\Gamma')\\ \frac{1}{2}\varphi_2(\mathbf{r}_p) & (p\in\Gamma'')\end{cases} \tag{10}$$

where $\varphi'=\varphi_1-\varphi_2$ and $\varphi''=-\varphi_2$. Considering Eqs. (8) and (9), differentiating Eq. (10) with regard to the normal on p yields

$$\frac{\partial\varphi_d(\mathbf{r}_p)}{\partial \mathbf{n}_p}+\int_{\Gamma}\varphi(\mathbf{r}_q)\frac{\partial^2 G(\mathbf{r}_p,\mathbf{r}_q)}{\partial \mathbf{n}_p\partial \mathbf{n}_q}d\Gamma = -ikA(\mathbf{r}_p)\varphi(\mathbf{r}_p)\quad(p\in\Gamma), \tag{11}$$

where $\Gamma=\Gamma'+\Gamma''$ and

$$\varphi(\mathbf{r}_p)=\begin{cases}\varphi'(\mathbf{r}_p) & (p\in\Gamma')\\ \varphi''(\mathbf{r}_p) & (p\in\Gamma'')\end{cases},\quad A(\mathbf{r}_p)=0\quad(p\in\Gamma''). \tag{12}$$

Note that Eq. (11) is in the same form as that for the analysis of a permeable thin surface in a free field. Discretizing Γ' and Γ'' with N' and N'' constant elements, respectively, and letting $N=N'+N''$, Eq. (11) yields

$$\frac{\partial\varphi_{d,i}}{\partial \mathbf{n}_i}+\sum_{j=1}^{N}\varphi_j\int_{\Gamma_j}\frac{\partial^2 G(\mathbf{r}_i,\mathbf{r}_q)}{\partial \mathbf{n}_i\partial \mathbf{n}_q}d\Gamma = -ikA_i\varphi_i\quad(i=1,\ldots,N), \tag{13}$$

where

$$\frac{\partial\varphi_{d,i}}{\partial \mathbf{n}_i}=\frac{\partial e^{ik\{\mathbf{h}(\theta)\cdot\mathbf{r}_i\}}}{\partial \mathbf{n}_i}=ik\{\mathbf{h}(\theta)\cdot\mathbf{n}_i\}e^{ik\{\mathbf{h}(\theta)\cdot\mathbf{r}_i\}}, \tag{14}$$

$$\frac{\partial^2 G(\mathbf{r}_i,\mathbf{r}_q)}{\partial \mathbf{n}_i\partial \mathbf{n}_q}=\frac{i}{4}\left[k\frac{\mathbf{H}_1^{(1)}(kr_{p_iq})}{r_{p_iq}}\cos(\mathbf{n}_i,\mathbf{n}_q)+\left\{k^2\mathbf{H}_0^{(1)}(kr_{p_iq})-2k\frac{\mathbf{H}_1^{(1)}(kr_{p_iq})}{r_{p_iq}}\right\}\times\cos(\mathbf{r}_{p_iq},\mathbf{n}_i)\cos(\mathbf{r}_{p_iq},\mathbf{n}_q)\right]. \tag{15}$$

$\mathbf{h}(\theta)=(\sin\theta,-\cos\theta)$ in Eq. (14) is a unit vector that indicates the direction of the plane wave and p_i in Eq. (15) is the center of the ith element. In Eq. (13), the fourth-order Gauss-Legendre quadrature is employed to calculate the integral of Eq. (15) for $i\neq j$. For $i=j$, the integral, which has hyper singularity, is estimated with Terai's method[40] for a region of length $\Delta\Gamma_j/3$ of center p_i and the Gauss-Legendre quadrature for the other regions, where $\Delta\Gamma_j$ means the length of the jth element. Potential differences φ_i on Γ' can be obtained by solving simultaneous equations of Eq. (13).

To avoid the non-uniqueness problem, which occurs at eigenfrequencies of Ω_3, the CHIEF method[38] is employed. Adding Eqs. (6) and (7) for p in Ω_3 yields

$$\varphi_d(\mathbf{r}_p)+\int_{\Gamma}\varphi(\mathbf{r}_q)\frac{\partial G(\mathbf{r}_p,\mathbf{r}_q)}{\partial \mathbf{n}_q}d\Gamma=0\quad(p\in\Omega_3), \tag{16}$$

which is discretized and approximately rewritten for M points in Ω_3 as

$$\varphi_{d,i}+\sum_{j=1}^{N}\varphi_j\int_{\Gamma_j}\frac{\partial^2 G(\mathbf{r}_i,\mathbf{r}_q)}{\partial \mathbf{n}_q}d\Gamma=0\quad(i=1,\ldots,M), \tag{17}$$

where

$$\varphi_{d,i} = e^{ik\{\mathbf{h}(\theta)\cdot\mathbf{r}_i\}}, \tag{18}$$

$$\frac{\partial G(\mathbf{r}_i,\mathbf{r}_q)}{\partial \mathbf{n}_q} = -\frac{i}{4}k\mathbf{H}_1^{(1)}(kr_{p_iq})\cos(\mathbf{r}_{p_iq},\mathbf{n}_q). \tag{19}$$

Equation (16) seems to be a redundant condition because both Eqs. (6) and (7) indicate that the potential in Ω_3 is zero and the number of equations and unknowns are already the same in Eq. (13) which can be solved as it is. However, by explicitly forcing the condition, spurious resonances in Ω_3 can be suppressed. Now Eqs. (13) and (17) form $N+M$ simultaneous equations for N unknowns, which are expressed as

$$\begin{bmatrix} ik\mathbf{Y}+\mathbf{H}' \\ \mathbf{H} \end{bmatrix}\mathbf{\Phi} = -\begin{bmatrix} \mathbf{\Phi}'_d \\ \mathbf{\Phi}_d \end{bmatrix}, \tag{20}$$

where $\mathbf{Y}$ is the diagonal admittance matrix which means the transmission characteristics of the MPP and is written by

$$\mathbf{Y} = \begin{bmatrix} A_1 & & 0 \\ & \ddots & \\ 0 & & A_N \end{bmatrix}, \tag{21}$$

$\mathbf{\Phi}=[\varphi_1,\ldots,\varphi_N]$ is the unknown potential vector, $\mathbf{\Phi}'_d=[\partial\varphi_{d,1}/\partial\boldsymbol{n}_1,\ldots,\partial\varphi_{d,N}/\partial\boldsymbol{n}_N]^T$ and $\mathbf{\Phi}_d=[\varphi_{d,1},\ldots,\varphi_{d,M}]^T$ are the direct component vectors where the superscript T indicates the transpose, $\mathbf{H}'$ and $\mathbf{H}$ are the matrices which mean interactions between the boundary elements and whose components are written by

$$\mathrm{H}'_{ij} = \int_{\Gamma_j}\frac{\partial^2 G(\mathbf{r}_i,\mathbf{r}_q)}{\partial\mathbf{n}_i\partial\mathbf{n}_j}d\Gamma, \quad \mathrm{H}_{ij} = \int_{\Gamma_j}\frac{\partial G(\mathbf{r}_i,\mathbf{r}_q)}{\partial\mathbf{n}_j}d\Gamma. \tag{22}$$

Representing the total matrix on the left-hand side of Eq. (20) by $\mathbf{A}$ and applying the least squares method yield

$$\mathbf{\Phi} = -(\mathbf{A}^H\mathbf{A})^{-1}\mathbf{A}^H\begin{bmatrix} \mathbf{\Phi}_d \\ \hat{\mathbf{\Phi}}_d \end{bmatrix}, \tag{23}$$

where H denotes the adjoint matrix.

Then the potential φ_a at an arbitrary point p can be numerically expressed as

$$\varphi_a(\mathbf{r}_p) = \varphi_{d,i} + \sum_{j=1}^{N}\varphi_j\int_{\Gamma_j}\frac{\partial G(\mathbf{r}_i,\mathbf{r}_q)}{\partial\mathbf{n}_q}d\Gamma \quad (p\in\Omega_{1,2,3}), \tag{24}$$

which is obtained by adding Eqs. (6) and (7).

C. MPP admittance

The transmission admittance ratio A_i in Eq. (13) is given by Maa's theory[1] as

$$A_i = \rho_0 c_0\left(\frac{P}{z_{\mathrm{resist}}+z_{\mathrm{react}}} - \frac{1}{i\omega\rho h}\right), \tag{25}$$

$$z_{\mathrm{resist}} = \frac{8\eta h}{(d/2)^2}\left(\sqrt{1+\frac{X}{32}}+\frac{\sqrt{2}dX}{8h}\right), \tag{26}$$

$$z_{\mathrm{react}} = -i\rho_0\omega h\left(1+\frac{1}{\sqrt{9+(X^2/2)}}+\frac{0.85d}{h}\right), \tag{27}$$

$$X = \frac{d}{2}\sqrt{\frac{\rho_0\omega}{\eta}}, \tag{28}$$

where ρ_0, c_0, and η are the density, sound speed, and viscosity coefficient of air, respectively. P, h, ρh, and d are the perforation ratio, thickness, surface density, and hole diameter of an MPP, respectively.

D. Dissipated energy ratio

This section derives the dissipated energy ratio, which is employed to evaluate the absorption performance of an MPP space absorber. The dissipated energy ratio means the difference between the absorption and transmission coefficients, $\alpha-\tau$, which can be calculated from the potential difference vector $\mathbf{\Phi}$ obtained from Eq. (23). The average value of $\alpha-\tau$ over all incident angles corresponds to the diffuse sound absorption coefficient measured in a reverberation chamber.[41] First, the dissipated acoustic energy in the jth element under a plane wave of incident angle θ is expressed as

$$W_j(\theta) = \frac{1}{2}\mathrm{Re}\{p_j\cdot v_j^*\}\Delta\Gamma_j, \tag{29}$$

where the asterisk denotes the complex conjugate. p_j is the sound pressure difference between the incident and transmitted sides of the MPP, which is expressed as

$$p_j = \rho_0\frac{\partial\varphi_j}{\partial t} = -i\rho_0\omega\varphi_j. \tag{30}$$

v_j is the particle velocity on the MPP surface, which is expressed as

$$v_j = -ikA_j\varphi_j. \tag{31}$$

Then the total dissipated energy can be written as

$$W_{ds}(\theta) = \sum_{j=1}^{N'}W_j(\theta) = \frac{(\rho_0\omega)^2}{2\rho_0 c_0}\sum_{j=1}^{N'}\mathrm{Re}\{A_j\}|\varphi_j|^2\Delta\Gamma_j. \tag{32}$$

Next the incident energy into a CMSA can be expressed as

$$W_{in}(\theta) = \frac{(\rho_0\omega)^2}{2\rho_0 c_0}\frac{l_1}{\pi}, \tag{33}$$

where l_1 is the perimeter of the circle. Consequently, considering the symmetric property of a CMSA, the dissipated energy ratio of a CMSA can be given by

$$\alpha-\tau = \frac{W_{ds}(\theta)}{W_{in}(\theta)} = \frac{\pi}{l_1}\sum_{j=1}^{N'}\mathrm{Re}\{A_j\}|\varphi_j|^2\Delta\Gamma_j. \tag{34}$$

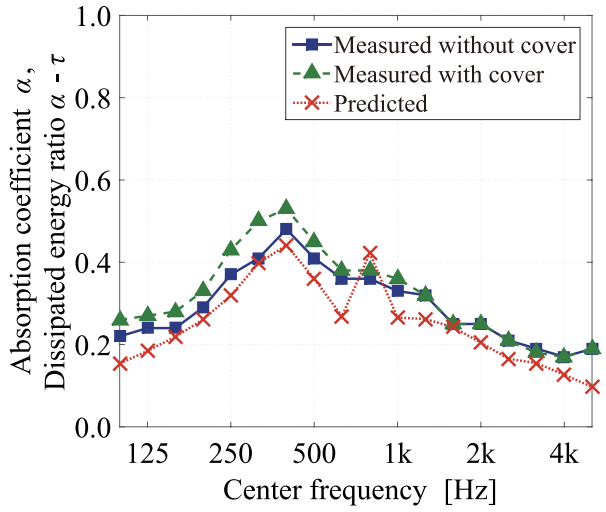

FIG. 3. (Color online) Comparison between the numerical and experimental results for a CMSA with a core with a 1-m perimeter of the CMSA and 50-mm diameter of the core.

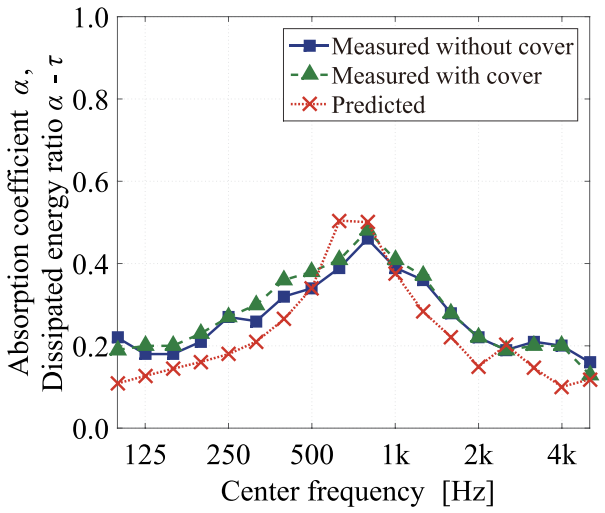

FIG. 5. (Color online) Comparison between the numerical and experimental results for a CMSA with a 165-mm diameter core and a 1-m CMSA perimeter.

III. COMPARISON

In this section, the numerical and experimental results[37] of CMSAs with cores are compared to discuss the prediction accuracy of the calculation method described in Sec. II. The perimeter of all CMSAs is 1 m (=318-mm diameter) and the MPP has a 0.5-mm hole diameter, 0.5-mm thickness, 0.785% perforation ratio, and 0.6-kg/m^2 surface density.

In the calculations, the MPP and core surface were, respectively, discretized into 240 straight-line elements. Therefore the longest element was about 1/240 m, which is less than 1/10 of the wavelength of air at 8000 Hz. CHIEF points were located in a lattice pattern with 1-mm intervals inside the core. The 1/3-octave band dissipated energy ratios were obtained by averaging the calculated energy with 1/24-octave intervals over each frequency range.

The measurement of the diffuse sound absorption coefficient in a reverberation chamber was carried out in compliance with JIS A 1409 [ISO 354 (Ref. 42) compatible]. The reverberation chamber is of volume 513 m^3 and surface area 382 m^2. A 1 m × 1 m MPP made of a transparent polycarbonate was formed into a cylindrical shape and then a cylindrical core made of acrylic or polyvinyl chloride was inserted in the center of it. The same 12 specimens were set and its absorption coefficients were measured in a reverberation chamber. To observe the difference due to the end condition of the top end, absorbers with an open end and absorbers with a closed end were measured, respectively. Although the measured results should be expressed as "absorption power of a unit surface area for a single specimen" instead of "absorption coefficient" when discussing these types of space sound absorbers, we herein treat "absorption power of a unit surface area for a single specimen" as absorption coefficient for convenience because the surface area of each specimen is 1 m^2 and the results for a single specimen did not change even if the number of specimens set in the reverberation chamber was changed.

Figures 3–6 compare the numerical and experimental results of the 1/3-octave band absorption characteristics of

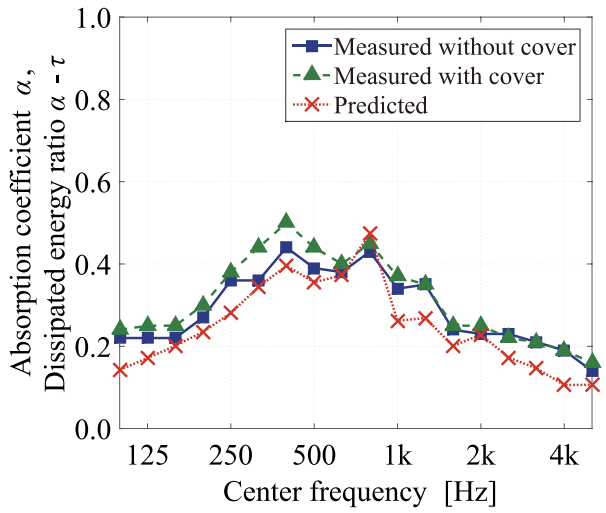

FIG. 4. (Color online) Comparison between the numerical and experimental results for a CMSA with a 100-mm diameter core and a 1-m CMSA perimeter.

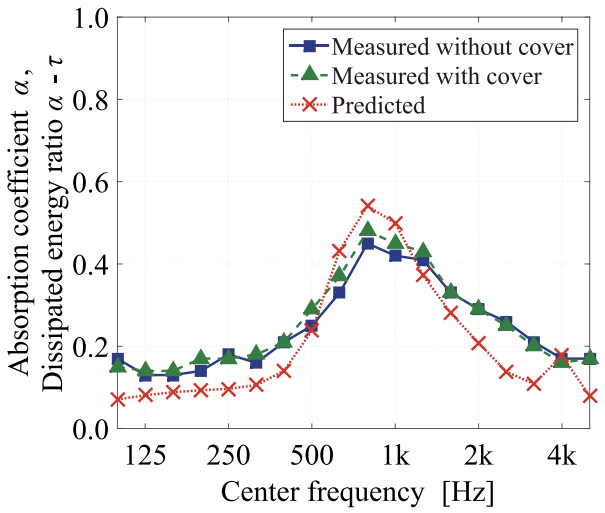

FIG. 6. (Color online) Comparison between the numerical and experimental results for a CMSA with a 215-mm diameter core and a 1-m CMSA perimeter.

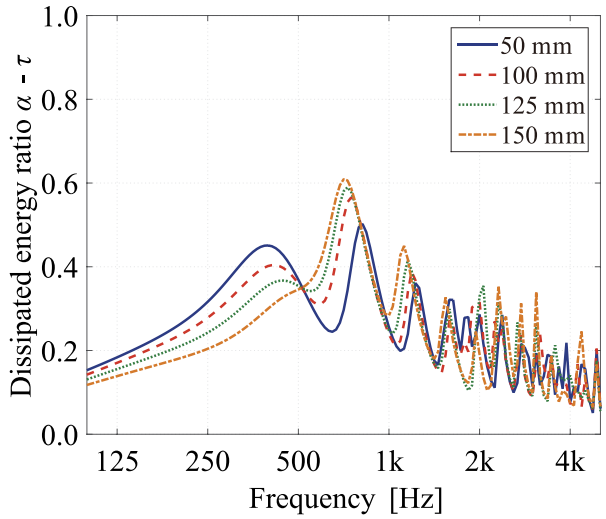

FIG. 7. (Color online) Transition of the absorption characteristics for a CMSA with core diameters ranging from 50 to 150 mm.

CMSAs with cores with 50-, 100-, 165-, and 215-mm diameters, respectively. The general absorption characteristics, including the peak frequency, can be predicted fairly well by the above calculation method.

The predicted results are however slightly lower than the measured ones except for the resonance peaks. In the two-dimensional calculations, the effects of resonances in the cross section of three-dimensional models become outstanding because oblique sound incidences of elevation do not cause disturbances. Therefore, the peaks in the predicted results tend to be higher than the measured ones. On the other hand, in the case without a cover, the oblique incidences from the open top-ends impinge on the internal sides of the MPPs. Thus, the dissipated energy in the experiments slightly exceeds the calculated value. In the case with a cover, additional resonances due to the closed region bounded by the MPP with a core and cover can occur, resulting in further energy dissipation.

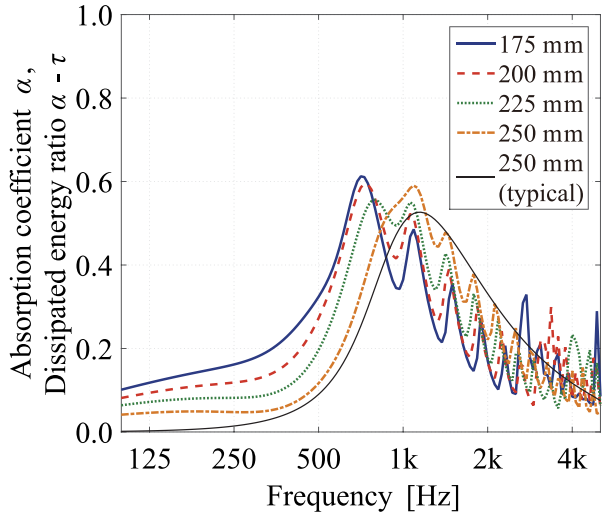

FIG. 8. (Color online) Transition of the absorption characteristics for a CMSA with core diameters ranging from 175 to 250 mm and for a typical MPP absorber with a 34-mm cavity depth.

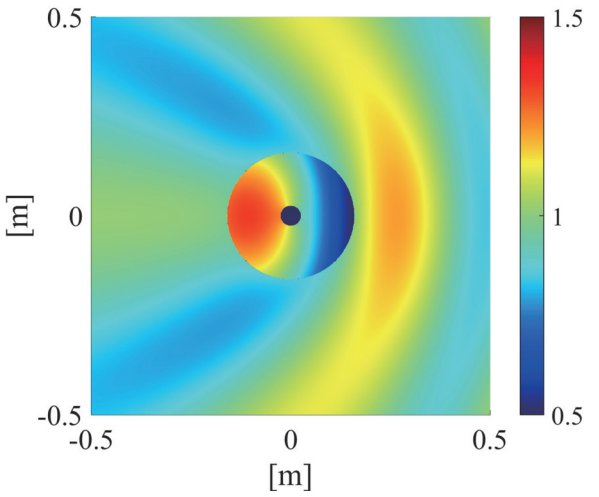

FIG. 9. (Color online) Distribution of the potential amplitude at 400 Hz.

Although some slight discrepancies, as stated above, are observed, the prediction accuracies for the general absorption performance and peak frequency are practically sufficient. However, three-dimensional numerical analyses are desired in order to realize more accurate predictions which makes it possible, for example, to discuss the effects of the cover quantitatively.

IV. PARAMETRIC STUDY

A parametric study with regard to the core size inside a CMSA was carried out to investigate the transition of the absorbing mechanism. The parameters of the CMSA were the same as those in Sec. III, but the core diameter was varied from 50 to 250 mm. Figures 7 and 8 show the numerical results of the absorption characteristics of CMSAs with different sized cores. In Fig. 8, the results of the random incidence absorption coefficient of a typical panel-like single-leaf MPP absorber are also shown. The MPP has the same parameters as those of CMSAs and the air cavity depth is set to 34 mm which corresponds to the normal distance between the MPP and the surface of the core with a 250-mm diameter.

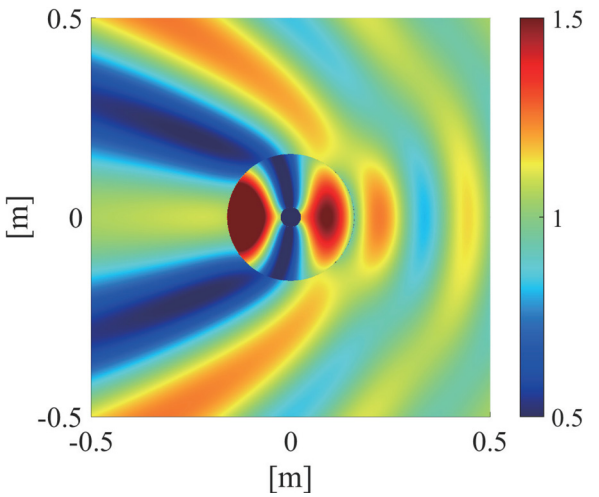

FIG. 10. (Color online) Distribution of the potential amplitude at 800 Hz.

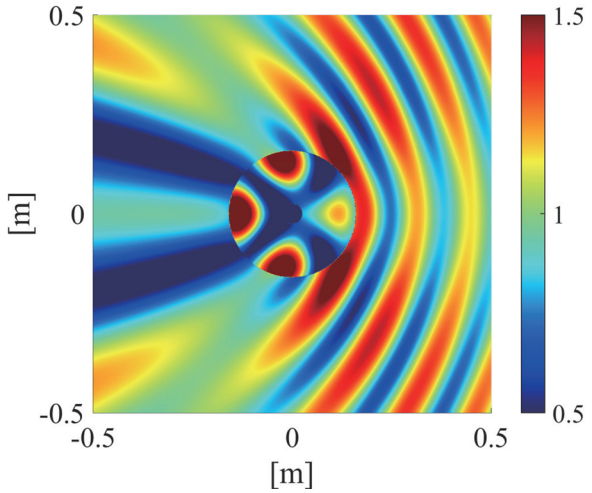

FIG. 11. (Color online) Distribution of the potential amplitude at 1250 Hz.

As the core diameter increases, the energy dissipation at low frequencies becomes weaker. When the core diameter is small, MPP leaves provide the appropriate acoustic resistance for low-frequency absorption.[31] However, as the core diameter increases, the resistance becomes too strong to absorb sound at low frequencies.

For a 50-mm core diameter, the absorption peaks observed around 400, 800, and 1250 Hz are caused by resonances due to the air cavities between MPPs, which have several path lengths and provide somewhat low but broad-band absorption characteristics. The distributions of potential amplitude obtained by Eq. (24) at 400, 800, and 1250 Hz are illustrated in Figs. 9, 10, and 11, respectively. These figures indicate the resonance modes at each frequency.

As the diameter increases, the first peak near 400 Hz becomes smaller and disappears at a 175-mm core diameter. On the other hand, the second and third peaks around 800 and 1250 Hz increase with core diameter. The second peak shows a maximum absorption when the diameter is 150 or 175 mm, but vanishes when the cavity diameter is 250 mm. At a 250-mm diameter, only the third peak survives, providing a rather high but selective sound absorption similar to a typical MPP absorber as shown in Fig. 8. This is because the core surface works as a rigid back wall for all azimuth incidences, reducing the variety of path lengths for a large core.

V. CONCLUSION

Herein the two-dimensional CHIEF method is employed to predict the absorption characteristics of a CMSA with a core. Comparing the numerical and experimental results confirms that the numerical method is sufficient for practical uses. In addition, a parametric study with regard to the core size shows a transition in the absorbing mechanism from one due to resonances between MPPs to one between the MPP and the core surface. These results demonstrate that a CMSA with a core can be used effectively by adjusting the core diameter to absorb sound at the target frequency and that the prediction method presented here is useful to design a CMSA with a core.

Further variations can be considered in a shape of an MPP space absorber. The authors are trying to investigate the acoustic characteristics of a variety of MPP space absorbers experimentally and theoretically, and will report them in the future.

ACKNOWLEDGMENTS

This work is in part supported by the research grant from the Obayashi Foundation.

[1]D. Y. Maa, "Theory and design of microperforated panel sound-absorbing constructions," Sci. Sin. **17**, 55–71 (1975).
[2]D. Y. Maa, "Microperforated-panel wideband absorber," Noise Control Eng. J. **29**, 77–84 (1987).
[3]D. Y. Maa, "Potential of microperforated panel absorber," J. Acoust. Soc. Am. **104**, 2861–2866 (1998).
[4]D. Y. Maa, "Practical single MPP absorber," Int. J. Acoust. Vib. **12**, 3–6 (2007).
[5]H. V. Fuchs, X. Zha, X. Zhou, and H. Drotleff, "Creating low-noise environments in communication rooms," Appl. Acoust. **62**, 1375–1396 (2001).
[6]X. Zha, H. V. Fuchs, and H. Drotleff, "Improving the acoustic working conditions for musicians in small spaces," Appl. Acoust. **63**, 203–221 (2002).
[7]J. Kang and M. W. Brocklesby, "Feasibility of applying micro-perforated absorbers in acoustic window systems," Appl. Acoust. **66**, 669–689 (2005).
[8]L. Huang, "Modal analysis of a drumlike silencer," J. Acoust. Soc. Am. **112**, 2014–2025 (2002).
[9]X. N. Wang, Y. S. Choy, and L. Cheng, "Hybrid noise control in a duct using a light micro-perforated plate," J. Acoust. Soc. Am. **132**, 3778–3787 (2012).
[10]X. Yu, L. Cheng, and J. L. Guyader, "Modeling vibroacoustic systems involving cascade open cavities and micro-perforated panels," J. Acoust. Soc. Am. **136**, 659–670 (2014).
[11]X. Yu and X. You, "Hybrid silencers with micro-perforated panels and internal partitions," J. Acoust. Soc. Am. **137**, 951–962 (2015).
[12]C. Yang, L. Cheng, and Z. Hu, "Reducing interior noise in a cylinder using micro-perforated panels," Appl. Acoust. **95**, 50–56 (2015).
[13]F. Asdrubali and G. Pispola, "Properties of transparent sound-absorbing panels for use in noise barriers," J. Acoust. Soc. Am. **121**, 214–221 (2007).
[14]C. Wang, L. Cheng, J. Pan, and G. Yu, "Sound absorption of a micro-perforated panel backed by an irregular-shaped cavity," J. Acoust. Soc. Am. **127**, 238–246 (2010).
[15]C. Wang and L. Huang, "On the acoustic properties of parallel arrangement of multiple micro-perforated panel absorbers with different cavity depths," J. Acoust. Soc. Am. **130**, 208–218 (2011).
[16]C. Yang, L. Cheng, and J. Pan, "Absorption of oblique incidence sound by a finite micro-perforated panel absorber," J. Acoust. Soc. Am. **133**, 201–209 (2013).
[17]Z. Xiaodan and F. Xiangqian, "Enhancing low frequency sound absorption of micro-perforated panel absorbers by using mechanical impedance plates," Appl. Acoust. **88**, 123–128 (2015).
[18]D. Chang, B. Liu, and X. Li, "An electromechanical low frequency panel sound absorber," J. Acoust. Soc. Am. **128**, 639–645 (2010).
[19]J. Tao, R. Jing, and X. Qiu, "Sound absorption of a finite micro-perforated panel backed by a shunted loudspeaker," J. Acoust. Soc. Am. **135**, 231–238 (2014).
[20]Y. Zhang, Y. J. Chan, and L. Huang, "Thin broadband noise absorption through acoustic reactance control by electro-mechanical coupling without sensor," J. Acoust. Soc. Am. **135**, 2738–2745 (2014).
[21]X. H. Duan, H. Q. Wang, Z. B. Li, L. K. Zhu, R. Chen, D. Y. Kong, and Z. Zhao, "Sound absorption of a flexible micro-perforated panel absorber based on PVDF piezoelectric film," Appl. Acoust. **88**, 84–89 (2015).
[22]J. S. Bolton and N. Kim, "Use of CFD to calculate the dynamic resistive end correction for microperforated materials," Acoust. Australia **38**, 134–139 (2010).
[23]T. Herdtle, J. S. Bolton, N. Kim, J. H. Alexander, and R. W. Gerdes, "Transfer impedance of microperforated materials with tapered holes," J. Acoust. Soc. Am. **134**, 4752–4762 (2013).
[24]L. Maxit, C. Yang, L. Cheng, and J. L. Guyader, "Modeling of micro-perforated panels in a complex vibro-acoustic environment using patch

transfer function approach," J. Acoust. Soc. Am. **131**, 2118–2130 (2012).
[25]T. Bravo, C. Maury, and C. Pinhède, "Sound absorption and transmission through flexible micro-perforated panels backed by an air layer and a thin plate," J. Acoust. Soc. Am. **131**, 3853–3863 (2012).
[26]T. Bravo, C. Maury, and C. Pinhède, "Vibroacoustic properties of thin micro-perforated panel absorbers," J. Acoust. Soc. Am. **132**, 789–798 (2012).
[27]T. Bravo, C. Maury, and C. Pinhède, "Enhancing sound absorption and transmission through flexible multi-layer micro-perforated structures," J. Acoust. Soc. Am. **134**, 3663–3673 (2013).
[28]L. Jaouen and F. X. Bécot, "Acoustical characterization of perforated facings," J. Acoust. Soc. Am. **129**, 1400–1406 (2011).
[29]A. Bockman, C. Fackler, and N. Xiang, "Bayesian-based estimation of acoustic surface impedance: Finite difference frequency domain approach," J. Acoust. Soc. Am. **137**, 1658–1666 (2015).
[30]K. Sakagami, M. Morimoto, and W. Koike, "A numerical study of double-leaf microperforated panel absorbers," Appl. Acoust. **67**, 609–619 (2006).
[31]K. Sakagami, T. Nakamori, M. Morimoto, and M. Yairi, "Double-leaf microperforated panel space absorbers: A revised theory and analysis," Appl. Acoust. **70**, 703–709 (2009).
[32]K. Sakagami, M. Yairi, and M. Morimoto, "Multiple-leaf sound absorbers with microperforated panels: An overview," Acoust. Australia **38**, 64–69 (2010).
[33]K. Sakagami, T. Nakamori, M. Morimoto, and M. Yairi, "Absorption characteristics of a space absorber using a microperforated panel and a permeable membrane," Acoust. Sci. Tech. **32**, 47–49 (2011).
[34]K. Sakagami, T. Oshitani, M. Yairi, E. Toyoda, and M. Morimoto, "An experimental study on a cylindrical microperforated panel space sound absorber," Noise Control Eng. J. **60**, 22–28 (2012).
[35]K. Sakagami, M. Yairi, E. Toyoda, and M. Toyoda, "An experimental study on the sound absorption of three-dimensional MPP space sound absorbers: Rectangular MPP space sound absorbers (RMSA)," Acoust. Australia **41**, 156–159 (2013).
[36]M. Toyoda, S. Kobatake, and K. Sakagami, "Numerical analyses of the sound absorption of three-dimensional MPP space sound absorbers," Appl. Acoust. **79**, 69–74 (2014).
[37]S. Fujita, K. Sakagami, M. Yairi, E. Toyoda, and M. Morimoto, "An experimental study of a cylindrical microperforated panel sound absorber with core," Noise Control Eng. J. **61**, 590–596 (2013).
[38]H. A. Schenck, "Improved integral formulation for acoustic radiation problems," J. Acoust. Soc. Am. **44**, 41–58 (1968).
[39]B. B. Baker and E. T. Copson, *The Mathematical Theory of Huygens Principle*, 3rd ed. (Chelsea, New York, 1987).
[40]T. Terai, "On calculation of sound fields around three dimensional objects by integral equation methods," J. Sound Vib. **69**, 71–100 (1980).
[41]K. Sakagami, T. Uyama, M. Morimoto, and M. Kiyama, "Prediction of the reverberation absorption coefficient of finite-size membrane absorbers," Appl. Acoust. **66**, 653–668 (2005).
[42]ISO 354:2003: Acoustics – Measurement of sound absorption in a reverberation room (International Organization for Standardization, Geneva, Switzerland).